# The Procapsid Binding Domain of $\phi$29 Packaging RNA Has a Modular Architecture and Requires 2′-Hydroxyl Groups in Packaging RNA Interaction†

Yun Fang,‡ Qi Cai,‡ and Peter Z. Qin*,‡,§

*Department of Chemistry and Department of Biological Sciences, University of Southern California, Los Angeles, California 90089-0744*

*Received November 28, 2004; Revised Manuscript Received May 3, 2005*

ABSTRACT: The $\phi$29 packaging RNA (pRNA) is an essential component in the $\phi$29 bacteriophage DNA packaging motor, the strongest biomolecular motor known today. Utilizing $Mg^{2+}$-dependent intermolecular base pairing interactions between two 4-nucleotide loops within the pRNA procapsid binding domain, multiple copies of pRNA form a ring-shaped complex that is indispensable for packaging motor function. To understand pRNA structural organization and pRNA/pRNA interaction, studies were carried out on pRNA closed dimers, the simplest functional pRNA complex believed to be the building blocks for assembling the oligomeric ring. Tertiary folding and interactions in various pRNA mutants were evaluated based on measured closed dimer affinity that is directly linked to the proper positioning of the interacting loops. The data revealed that the procapsid binding domain contains two autonomous modules that are capable of interacting noncovalently to form a fully active species in pRNA/pRNA interaction. Deleting the 2′-hydroxyl groups in one of the interacting loops weakens the dimer affinity by 125-fold, suggesting potential tertiary interactions involving these 2′-hydroxyl groups. The results provide evidence that nonbase functional groups are involved in pRNA folding and interaction and lead to a simple model that describes the pRNA monomer configuration in terms of three arms spanning a hinge. The functional constructs developed here will aid biophysical and biochemical investigations of pRNA structure and function, as well as developments of pRNA-based technology for nanoscience and gene therapy.

During maturation of many linear double-stranded DNA viruses, the linear DNA genome is condensed to a near-crystalline state inside a protein capsid (procapsid) utilizing energy generated from ATP hydrolysis (*1*). The process of condensing the DNA is carried out by the packaging motor, and it is believed that different double-stranded DNA bacteriophages all use the same DNA-packaging mechanism (*2*−*5*). One of the best studied packaging systems is bacteriophage $\phi$29, a representative of the $\phi$29 family of bacteriophages (see reviews *5*, *6*). It has been shown that the $\phi$29 packaging motor is one of the strongest biological motors known today, capable of generating forces that are 2- ∼ 8-fold higher than other motors such as myosin and RNA polymerase (*7*). The mechanism of $\phi$29 packaging motor function is not known, although several mechanistic models have been proposed (*5*, *8*−*11*).

The $\phi$29 packaging motor is a protein/RNA complex, and the RNA component, called the packaging RNA (pRNA[1]), is required for motor function both in vivo and in vitro (*12*). In in vitro DNA packaging, a 120-nucleotide (120-nt) pRNA is required and sufficient for full-packaging activity (*12*). Extensive studies have revealed that a pRNA monomer folds into two separate domains (*5*, *6*) (Figure 1A). One is called the DNA translocation domain, which is essential for DNA packaging yet dispensable for procapsid binding (*13*, *14*). The other is called the procapsid binding domain and is responsible for pRNA binding to the capsid, as well as pRNA/pRNA interaction (*13*, *15*−*23*). Within the procapsid binding domain reside two stretches of sequences, termed R-loop and L-loop, that are complementary to each other (*18*, *19*) (Figure 1A). Through $Mg^{2+}$-dependent, intermolecular R/L loop base-pairing interactions, multiple copies of pRNAs form a ring-shaped oligomeric complex that is believed to be the active form in motor function (*18*, *19*). Neither specific base sequence nor intramolecular R/L loop complementarity is required (*18*, *19*). The exact composition of the pRNA oligomer is still under debate: biochemical studies strongly indicate that the active pRNA complex is a hexamer (*18*, *19*), while microscopy studies show that the pRNA forms either a hexamer (*24*) or a pentamer (*9*).

It has been shown that the ATPase activity of the packaging motor is strongly stimulated by pRNA (*25*), and a recent report suggested direct interaction between pRNA and ATP (*26*). Therefore, pRNA is likely not limited to being a passive structural component of the packaging motor. Understanding the structure of pRNA and pRNA motions during DNA packaging is one of the critical steps in unveiling the mechanism of the packaging motor. In addition,

† Research reported here was supported by the Petroleum Research Fund (PRF No. 39623-G4), the Zumberge Research Fund, and a startup fund from the University of Southern California.

* To whom correspondence should be addressed: University of Southern California, LJS-251, 840 Downey Way, Los Angeles, CA 90089-0744. Tel, (213) 821-2461; fax, (213) 740-0930; e-mail, pzq@usc.edu.

‡ Department of Chemistry.

§ Department of Biological Sciences.

[1] Abbreviations: pRNA, $\phi$29 packaging RNA; MOPS, 3-[*N*-morpholino]propanesulfonic acid; Tris, 2-amino-2-(hydroxymethyl)-1,3-propanediol; EDTA, ethylenediaminetetraacetic acid; DTT, Dithiothreitol; TBM buffer, 89 mM Tris-HCl (pH 7.6), 0.2 M boric acid, and 5 mM $MgCl_2$.

10.1021/bi0475020 CCC: $30.25 
Published on Web 06/09/2005

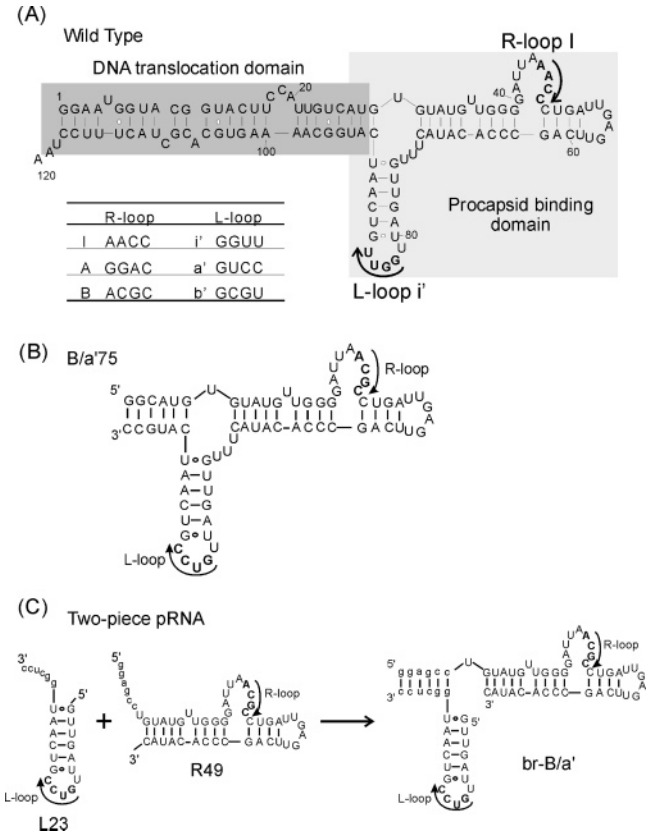


FIGURE 1: (A) Sequence and secondary structure of the wild-type, full-length pRNA molecule. The DNA translocation domain and the procapsid binding domain are each indicated by gray boxes. The R-loop and L-loop that are utilized for intermolecular oligomer formation are marked by arrows. The loop sequences of wild-type and mutant pRNAs, together with their letter designations, are listed in the inset. (B) Sequence and secondary structure of the B/a′75 molecule. Compared to the full-length pRNA, B/a′75 has the DNA translocation domain truncated to a six-base pair duplex. The sequence of the terminal three base pairs were mutated to facilitate T7 in vitro transcription. (C) Sequence and secondary structure of the two-piece br-B/a′ RNA.

pRNAs have been utilized in ribozyme delivery (*27*) and constructing artificial nanostructures (*28*, *29*), and information on pRNA structure and interaction is critical for these developments.

Currently, information on the tertiary structure of pRNA is limited, and much less is known about the conformational changes of pRNA during DNA packaging. The intermolecular R/L loop interaction, identified through extensive sequence mutational analyses, is the only known pRNA/pRNA interaction element (see reviews *5*, *6*). Chemical probing and photocross-linking studies have identified a small number of short-range structural constraints (*21*, *30*−*33*), and several computational models of pRNA in various oligomeric states have bee proposed (*19*, *23*, *34*). However, more constraints, both short-range and long-range, are necessary to determine the pRNA structure, and constructs and techniques that can provide time-dependent structural information are required to probe how the pRNA conformations change during DNA packaging.

As a step toward understanding the pRNA structural organization and pRNA/pRNA interaction, we are interested in studying the simplest, stable, functionally relevant pRNA/pRNA complexes, closed dimers of pRNA that contain two sets of intermolecular R/L interactions. Closed dimers of pRNA form in the absence of proteins and serve as building blocks that are recognized by the procapsid in assembling the pRNA ring (*22*). In studies of procapsid binding and DNA packaging, closed dimers show higher activity than that of open dimers (only one R/L interaction), and monomers are unable to compete with dimers for procapsid binding (*22*). Furthermore, full activity is retained in covalently linked closed dimers, where the two monomeric units are connected via either photocross-linking or linker RNA sequences (*22*). On the basis of these data, it has been proposed that pRNA closed dimers independently fold into a specific configuration that is a prerequisite for procapsid binding, pRNA ring formation, and pRNA function.

Although the configuration of the closed dimer likely differs from that of the active pRNA complex (either a hexamer or a pentamer), they share an overarching structural feature, they utilize multiple intermolecular R/L loop pairing interactions to form closed ring-shaped entities. Studying the closed dimer will reveal how pRNA functionalities are utilized to construct closed ring-shaped complexes. Such findings might be applicable to the active pRNA hexamer or pentamer. For example, photocross-linking and chemical modification studies in pRNA closed dimers have provided evidence that the L-loop hairpin might flip around a flexible $U_{72}U_{73}U_{74}$ loop (*32*). Analyzing the roles of pRNA mutations in the context of DNA-packaging activity has revealed a requirement of flexibility in the same $U_{72}U_{73}U_{74}$ loop (*16*, *35*). This suggests that proposed movements around the $U_{72}U_{73}U_{74}$ loop, revealed in closed dimer studies, play a role in the function of the active pRNA ring. Therefore, the closed dimer is a valid model system for acquiring information that is relevant to pRNA function.

In this study, the dissociation constant ($K_d$) and the standard state free energy of formation ($\Delta G°$) for a pRNA closed dimer were determined using a native gel assay. Closed dimer formation is linked to the correct tertiary folding of pRNA, as it requires proper positioning of two pairs of intermolecular R/L loops and incurs strong $Mg^{2+}$ dependence (*22*). Therefore, the measured $K_d$ and $\Delta G°$ values were utilized to evaluate tertiary folding and interactions in a variety of pRNA mutants. The data indicate that the procapsid binding domain of pRNA can be broken into two separate molecules, each containing one of the interacting loops. The submodules interact without covalent linkage to fold into a fully active configuration for pRNA/pRNA interaction. This modular organization of the pRNA led to a simple three-arms-around-a-hinge model for pRNA monomer configuration. Utilizing this functionally active two-piece pRNA system, we show that deleting the 2′-hydroxyl groups in one of the interacting loops weakens the dimer affinity by 125-fold. This provides evidence that nonbase functionalities participate in the structure and function of pRNA. The results suggest potential tertiary interactions involving these 2′-hydroxyl groups and demonstrate that the functionally active pRNA constructs reported here provide a valuable system for probing pRNA structure and function.

## MATERIALS AND METHODS

*Materials.* Plasmid pT7temp contains the T7 promoter followed by one copy of the wild-type 120-nt pRNA

Table 1.

(A) DNA Primers Used for Mutating pRNA Loop Sequences

| intended mutations | | primer sequence[a,b] |
|---|---|---|
| R-loop | (A) 5′ GGAC | 5′ GTC ATG TGT ATG TTG GGG ATT A*GG ACC* TGA TTG AGT TCA GCC CAC |
| | (B) 5′ACGC | 5′ GTG TAT GTT GGG GAT TA*A CGC* CTG ATT GAG TTC AGC CCA C |
| L-loop | (a′) 5′GTCC | 5′ CC CAC ATA CTT TGT TGA TT*G TCC* GTC AAT CAT GGC AAA AGT GCA C |
| | (b′) 5′GCGU | 5′ CC CAC ATA CTT TGT TGA TT*G CGT* GTC AAT CAT GGC AAA AGT GCA C |

(B) PCR Primers for Generating Linearized DNA Plasmids for in Vitro Transcription

| target pRNA | primer sequences |
|---|---|
| full-length (120 nt) | forward: 5′ TAA TAC GAC TCA CTA TAG GAA TGG TAC GGT AC<br>backward: 5′ TTA GGA AAG TAG CGT GCA CTT TTG |
| B/a′75 | forward: 5′ TAA TAC GAC TCA CTA TAG GCA TGT GTA TGT TGG GG<br>backward: 5′ GGC ATG ATT GAC GGA C |

[a] Only the sense primer sequences are shown. [b] The resulting loop sequences are in italics.

sequence (*35*) and was kindly provided by Dr. Peixuan Guo at Purdue University. T7 RNA polymerase was over-expressed and purified according to a published protocol using a cell line kindly provided by Dr. Anna M. Pyle at Yale University (*36, 37*). All chemicals and reagents were molecular biology grade.

*Nomenclature.* An intact pRNA molecule is identified as R/l′*n*, with *n* representing the RNA length. R designates the R-loop sequence and is assigned an upper case letter (i.e., A, B, ...). l′ designates the L-loop sequence and is assigned a lower case letter with a prime (i.e., a′, b′, ...) (*18*). The same set of letters (i.e., A/a′) designates complementary sequences in the R/L loop, while different letters indicate lack of sequence complementarity. For example, the wild-type pRNA is designated I/i′120. The loop sequences and their corresponding letter designations used in this study are listed in Figure 1A (inset).

*DNA Plasmids and Transcription Templates.* Plasmids containing one copy of the full-length, 120-nt pRNA with mutated R-loops or L-loops were constructed using the QuikChange site-directed mutagenesis kit (Stratagene, Inc.) with plasmid pT7temp as the starting template. Mutation primers are listed in Table 1A. The presence of mutation was confirmed by DNA sequencing.

Linearized DNA templates for in vitro transcription were generated by PCR, using primers listed in Table 1B. PCR reactions were carried out in a PTC-100 peltier thermal cycler (MJ research), in a mixture (100 $\mu$L) containing 100 pg of Hind III-linearized plasmid, 1.0 $\mu$M of each primer, 0.25 mM of each dNTP, 2.5 mM $MgCl_2$, 2.5 units of *Taq* polymerase (Promega), 50 mM KCl, 10 mM Tris-HCl (pH 9.0 at 25 °C), and 0.1% Triton X-100. Reactions proceeded for 30 cycles according to the following scheme: 30 s at 94 °C, 30 s at 55 °C, and 1 min at 72 °C. Reactions were judged successful by the appearance of only one band with the correct size when analyzed on a 4% agarose gel. For each template, a total of 10 reactions were carried out, the solutions were combined, and the unincorporated primers and dNTPs were removed using Ultrafree-30 centrifugal filters (30K molecular cutoff, Millipore, Inc.). *Taq* polymerase was removed by phenol extraction. DNA templates were recovered by ethanol precipitation, and re-suspended in the ME buffer (10 mM MOPS, pH 6.5, and 1 mM EDTA). Template concentrations were calculated from the absorbance at 260 nm measured in a Beckman DU800 UV-Vis spectrometer (1 OD = 50 ng/$\mu$L).

*RNA Synthesis.* Full-length pRNAs and the B/a′75 RNA (Figure 1 A,B) were generated by T7 in vitro transcription using linearized DNA plasmid templates (*38, 39*). Transcription reaction mixtures (400 $\mu$L) contained 10 $\mu$g of linearized DNA plasmid template, 0.75 mM of each NTP, 150 units of T7 RNA polymerase, 40 mM Tris-HCl (pH 8.0), 50 mM NaCl, 15 mM $MgCl_2$, 30 mM DTT, and 2 mM spermidine. After incubation at 37 °C for 3 h, EDTA was added to a final concentration of 20 mM, and RNA was recovered by ethanol precipitation.

For the two-piece br-B/a′ pRNA system (Figure 1C), the sequence of R49 is 5′ gga gcc UGU AUG UUG GGG AUU AAC GCC UGA UUG AGU UCA GCC CAC AUA C, with the R-loop sequence underlined, and lower case letters representing the sequence forming the clamping duplex. The sequence of the L23 RNA is 5′ GUU GAU UGU CCG UCA AUg gcu cc, with the L-loop sequence underlined. The dL23 sequence is 5′ GUU GAU UdGdU dCdCG UCA AUg gcu cc, with the L-loop sequence (underlined) changed to deoxyribonucleotides. The L18 RNA, where the clamping sequence is deleted, has the sequence 5′ GUU GAU U*GU CC*G UCA AUg. These RNAs were generated by solid-phase chemical synthesis (Dharmacon, Inc., Lafayette, CO) and deprotected following protocols provided by the vendor.

RNA was purified using denaturing polyacrylamide gel electrophoresis (PAGE) and quantified according to absorbance at 260 nm, using an extinction coefficient of 10 000 $M^{-1}$ $cm^{-1}$ per nucleotide. The sequence of the transcribed RNA was verified using phosphorothioate mapping (*40*).

*Radiolabeling at the 5′ Terminus of RNA.* RNA molecules generated by in vitro transcription contain a 5′ triphosphate group and were dephosphorylated using calf intestinal alkaline phosphatase following the protocol provided by the vendor (Promega). RNA containing a 5′-OH group was kinased in the presence of [$\gamma$-$^{32}$P]ATP. The reaction mixture contained 10 pmol of RNA, 1 unit of T4 polynucleotide kinase, 40 mM Tris-HCl (pH 7.5 at 25°C), 10 mM $MgCl_2$, 5 mM DTT, and 0.1 mCi [$\gamma$-$^{32}$P]ATP. After incubation at 37 °C for 30 min, RNA was purified by PAGE.

*Analyzing pRNA Dimer and Trimer Formation by Native Gels.* Binding was measured in the TBM buffer. The individual RNA was first heated at 95 °C for 1 min, cooled at room temperature for 2 min, and incubated in the TBM buffer for 2 min at room temperature. In binding measurements involving the two-piece br-B/a′ pRNA, R49 and L23 were mixed during 95 °C heating and treated as one

individual RNA in subsequent steps. After preincubation, the RNAs were mixed, and incubation continued in the TBM buffer at 17 °C for 1 h. The final volume of the reaction mixture was 5 $\mu$L and included 5% (v/v) glycerol and 0.03% (v/v) xylene cyanol. The pRNA monomer, dimer, and trimer were separated according to their mobilities on a 10% native polyacrylamide gel, prepared and ran in the TBM buffer. Temperature during electrophoresis was controlled using a circulating water pump, adjusted so that the temperature recorded at the outside plate was set at the desired reaction temperature. The RNA bands were visualized by either ethidium bromide staining or autoradiography.

*Determinations of Dimer Dissociation Constants ($K_d$) and Standard State Free Energy of Formation ($\Delta G°$).* Dimer affinity was determined by measuring the percentage of dimer formed when a fixed, trace amount of radiolabeled pRNA1 (*p1) was combined with various concentrations of unlabeled pRNA2 (p2). The populations of monomer and dimer were separated on native gels and quantified using a Storm 860 phosphorimager (Molecular Dynamics). The amount of each band was determined by the number of counts within a box drawn round the band. Background correction at each box was determined by multiplying the box size with a background-per-unit-area value determined at an empty region of the gel.

Radiolabeled *A/b′120 was utilized as the trace probe in most studies, in which case, only monomer and dimer can be observed on the gel. The fraction of dimer, $\alpha$, at each p2 concentration was calculated by dividing the counts of the dimer to the sum of dimer and monomer. Under the condition $[*p1]_0 \ll [p2]_0$, the dissociation constant, $K_d$, was determined by fitting the data to the following equation using the program Kaleidagraph (Synergy, PA):

$$\alpha = \frac{[p2]_0}{[p2]_0 + K_d} \quad (1)$$

where $K_d = [*p1][p2]/[\text{dimer}]$, and $[p2]_0$ is the total concentration of pRNA2.

In studies involving the two-piece B/a′ RNA, radiolabeled *L23 was also utilized as the probe. Trace amount of *L23 was first combined with a fixed amount of R49 (0.1 $\mu$M) to yield a constant concentration of *br-B/a′. Binding was measured with varying concentrations of A/b′120. Three bands were observed on the gel, corresponding to *L23, *br-B/a′, and dimer, respectively. $K_d$ was determined by fitting the data to the following equation:

$$\alpha' = \frac{\dfrac{[\text{dimer}]}{[*\text{L23}] + [*\text{br-B/a'}] + [\text{dimer}]}}{\dfrac{[\text{dimer}] + [*\text{br-B/a'}]}{[*\text{L23}] + [*\text{br-B/a'}] + [\text{dimer}]}} = \frac{[\text{dimer}]}{[*\text{br-B/a'}] + [\text{dimer}]} = \frac{[\text{A/b'120}]_0}{[\text{A/b'120}]_0 + K_d} \quad (2)$$

where $K_d = [*\text{br-B/a′}][\text{A/b′120}]/[\text{dimer}]$, and $[\text{A/b′120}]_0$ is the total concentration of A/b′120. This analysis is valid if individually neither L23 nor R49 interacts with A/b′120, which was shown to be true in control experiments. Similar analysis was carried out with *dL23, where the L-loop is mutated to deoxyribonucleotides.

The standard state free energy of dimer formation was calculated as

$$\Delta G° = -RT \ln(1/K_d) \quad (3)$$

where $R$ is the gas constant and $T$ is the absolute temperature ($T = 290$ K in this work).

## RESULTS

*Quantitative Analyses of Interactions between Full-Length pRNAs.* To quantitatively study pRNA/pRNA interaction, it is essential to control the formation of pRNA oligomers. In the in vitro studies, the wild-type pRNA (I/i′120) exists as a mixture of species in different oligomeric states (*18*, *19*). Previous studies have successfully overcome the uncontrollable oligomerization by mutations that destroy intramolecular sequence complementarity between the R and L loops (*18*, *19*). The same strategy was utilized in this report. The sequences of the R and L loops utilized in this study are shown in Figure 1A. These sequences have been shown in previous studies to be fully functional in DNA packaging (*18*, *19*). To demonstrate our capability to control pRNA interactions, previously reported experiments (*18*, *19*, *22*) were repeated to show dimer formations between full-length pRNAs (Figure 2A). When equal amounts of A/b′120 and B/a′120 were mixed in the presence of 5 mM $Mg^{2+}$, a band with retarded mobility was observed on the native gel (Figure 2A, lane 3). According to reports in the literature (*22*), this band represents a pRNA closed dimer as it contains two complementary R/L loop interactions (A||a′ and B||b′). As previously reported, detection of a stable dimer species on the native gel requires two sets of complementary R/L interactions (Figure 2A, lanes 4 and 5) (*18*, *19*, *22*). In the following text, "dimer" refers to a pRNA closed-dimer.

The native gel assay was then extended for quantitatively analysis of pRNA dimer formation. In these studies, a trace amount of radiolabeled A/b′120 (*A/b′120) was mixed with varying concentrations of B/a′120, and the resulting monomers and dimers were separated using the native gel (Figure 2B). The fractions of dimer at each B/a′120 concentration were quantified, and the data were fit to eq 1 to yield a dissociation constant, $K_d$ (Figure 2C). Under 5 mM $Mg^{2+}$, a $K_d$ of 21.7 ± 8.2 nM was determined, corresponding to a $\Delta G°_{17°C}$ of −10.2 kcal/mol (Table 2). Because closed dimer formation requires proper positioning of the R and L loops, it is linked to the formation of the proper pRNA tertiary structure. The $K_d$ and $\Delta G°_{17°C}$ values of dimer formation provide a quantitative indicator for evaluating tertiary folding of pRNA mutants and can be used to reveal the roles of various pRNA subdomains in tertiary folding and interaction.

*Truncation of the DNA Translocation Domain Does Not Affect pRNA Dimer Affinity.* A large body of data has shown that the DNA translocation domain and the procapsid binding domain (which includes the R and L loops) constitute two nonoverlapping units (Figure 1A) (see reviews *5*, *6*). Particularly, previous studies have shown that a 75-nt pRNA mutant, where the DNA translocation domain was truncated, is capable of interacting with procapsid and pRNA (*22*). To further test the utility of the measured $K_d$ and $\Delta G°$ values for evaluating pRNA folding and interaction, a 75-nt molecule (B/a′75, Figure 1B) with a truncated DNA translocation domain was constructed from the full-length B/a′120,

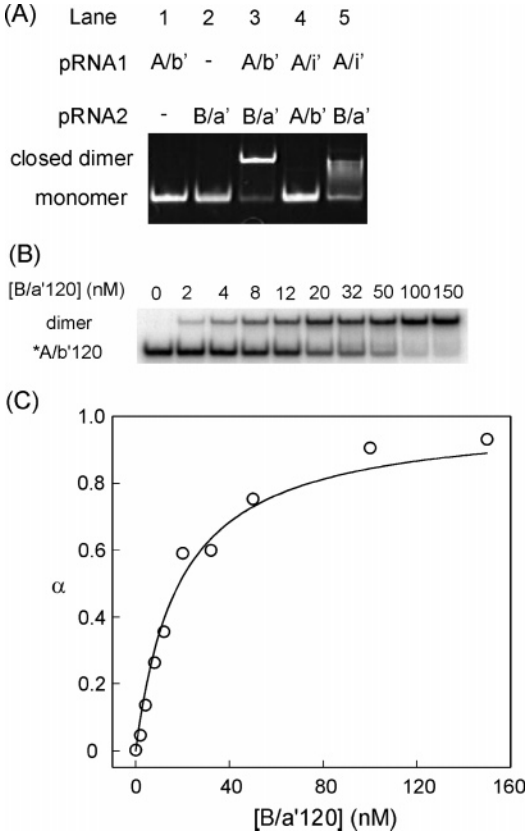


FIGURE 2: Dimer formation in full-length pRNAs. (A) A native gel showing controlled dimer formation between unlabeled RNAs. Reactions were carried out in 5 mM $Mg^{2+}$. In each lane, the total RNA concentration was 3.0 $\mu$M, with an equal molar ratio of each RNA in reactions containing two RNAs. Lanes 1 and 2 showed that the individual A/b′120 and B/a′120, which lack base-pairing interactions between the R/L loops, migrated as monomers with equal mobility. Lane 3 showed mixing equal amounts of A/b′120 and B/a′120 led to a retarded band that represents a pRNA closed dimer with two complementary R/L loop interactions (A||a′ and B||b′). Lane 4 showed no interaction between pRNAs lacking complementary R/L loops, and lane 5 showed that a possible open-dimer species with only one R/L interaction (A||a′) migrated abnormally on a native gel. (B) An autoradiograph with signal derived from radiolabeled *A/b′120. As concentrations of unlabeled B/a′120 increased, monomeric A/b′120 was observed to shift into dimer. (C) Quantitative binding analysis. The fractions of dimer, α, were calculated and plotted against the concentrations of B/a′120. Fitting the shown data to eq 1 yielded a $K_d$ value of 20.7 nM. Lowing the concentration of $^{32}$P-labeled A/b′120 by 5-fold did not alter the observed $K_d$, suggesting it is valid to apply eq 1.

and dimer affinity between B/a′75 and full-length A/b′120 was measured. B/a′75 was chosen in these studies because the truncated RNA preserves the wild-type secondary structure.

The B/a′75 molecule formed a dimer upon addition of A/b′120 (Figure 3A). The $K_d$ between B/a′75 and A/b′120 was determined to be 24.8 ± 1.0 nM, corresponding to a $\Delta G°_{17°C}$ of −10.1 kcal/mol (Figure 3B, Table 2). Within errors, these values are the same as that of the full-length B/a′120. This suggests that truncation of the DNA translocation domain has no effect on pRNA dimer formation and indicates the procapsid binding domain folds and interacts independently from the DNA translocation domain. This is consistent with previous reports (*15*, *17*, *22*) and supports the notion that the measured $K_d$ and $\Delta G°_{17°C}$ values serve as indicators for pRNA tertiary folding and interaction.

Table 2: Measured Parameters for pRNA Dimer Formation[a]

| *pRNA1[b] | pRNA2 | $K_d$ (nM)[c] | $\Delta G°_{17°C}$[d] (kcal/mol) | $\Delta\Delta G°_{17°C}$[e] (kcal/mol) |
|---|---|---|---|---|
| *A/b′120 | B/a′120 | 21.7 ± 8.2 | −10.2 ± 0.22 | − |
| *A/b′120 | B/a′75 | 24.8 ± 1.0 | −10.1 ± 0.02 | 0.1 |
| *A/b′120 | br-B/a′ | 48.9 ± 13.8 | −9.7 ± 0.10 | 0.5 |
| *br-B/a′ | A/b′120 | 68.0 ± 8.2 | −9.5 ± 0.07 | 0.7 |
| average[f] | | 58.5 ± 9.6 | −9.6 ± 0.09 | 0.6 |
| *A/b′120 | br-B/da′ | 6885 ± 1584 | −6.8 ± 0.13 | 3.4 |
| *br-B/da′ | A/b′120 | 7684 ± 733 | −6.8 ± 0.05 | 3.4 |
| average[f] | | 7285 ± 400 | −6.8 ± 0.03 | 3.4 |

[a] Measurements were carried out at 17 °C as described in Materials and Methods. [b] Radiolabeled RNAs used as trace probes. [c] Errors obtained from multiple measurements. [d] Errors calculated from propagating errors in $K_d$ measurements. [e] $\Delta\Delta G°_{17°C} = \Delta G°_{17°C}$ (mutant) − $\Delta G°_{17°C}$ (B/a′120). [f] Averaged from the two assays using different trace radiolabeled probes.

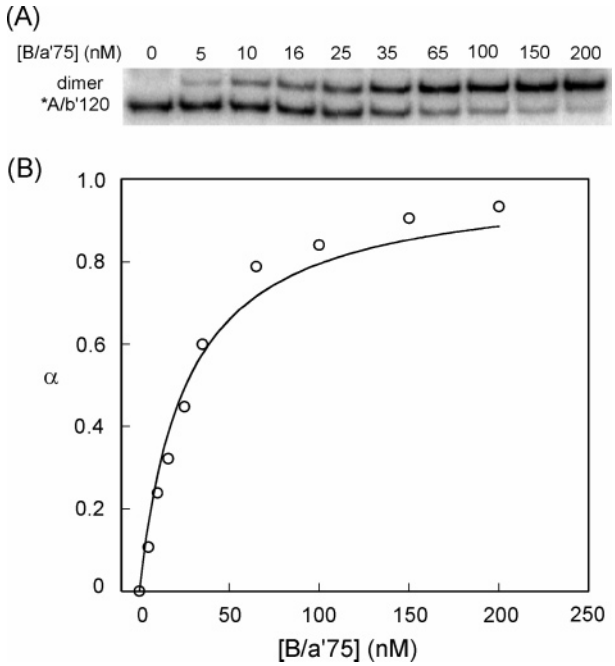


FIGURE 3: Dimer formation with B/a′75. (A) An autoradiograph with signal derived from radiolabeled *A/b′120. Increasing amount of dimer was formed as the concentration of unlabeled B/a′75 increased. (B) Quantitative analyses of the concentration dependence in the fractions of dimer, α. The data shown here yielded a $K_d$ value of 25.9 nM for B/a′75.

*Two Autonomous Folding Modules within the Procapsid Binding Domain.* Data presented above indicate that a 75-nt pRNA containing the R-loop and L-loop is fully capable of dimer formation. It was then interesting to further study the architecture of this minimized pRNA. For this purpose, a two-piece pRNA construct, designated br-B/a′ (for "broken" B/a′), was developed. The B/a′75 RNA was split at the $U_{72}U_{73}U_{74}$ loop to create a R49 molecule that includes the R-loop and a L23 molecule that includes the L-loop (Figure 1C). The two molecules interact noncovalently via a six-nucleotide duplex that serves as an anchor as well as a truncated helical DNA translocation domain (Figure 1C).

Native gel binding assays were carried out to test whether br-B/a′ assembles as designed (Figure 4A). Radiolabeled *L23 was observed to interact with R49 to form a species that has a similar mobility as that of the intact B/a′75 (Figure 4A, lanes 3 and 4), indicating successful assembly of br-B/

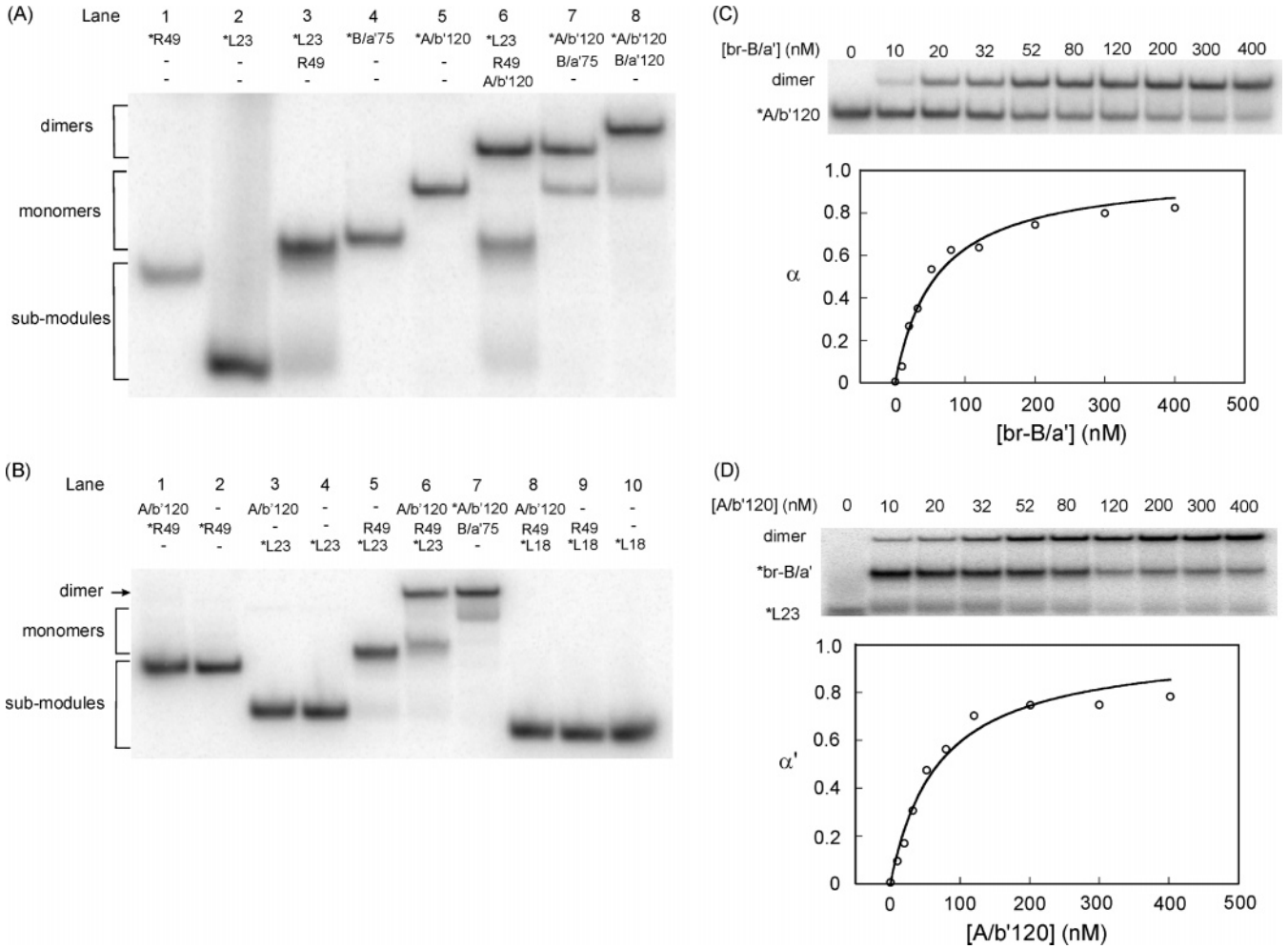


FIGURE 4: Dimer formation with the two-piece br-B/a′ pRNA. (A) br-B/a′ assembly as detected by native gel. "*" indicates radiolabeled RNAs. All unlabeled RNAs were at 0.1 $\mu$M. Lane 3 showed that the reconstituted br-B/a′75 species migrated with similar mobility as that of an intact B/a′75 (lane 4) and was retarded as compared to *L23 (lane 2) and *R49 (lane 1). Lane 6 showed mixing br-B/a′75 and A/b′120 resulted in a retarded band that migrated the same as the dimer formed between the intact B/a′75 and A/b′120 (lane 7). (B) Functions of br-B/a′ require the clamping duplex. In each lane, 2.0 $\mu$M each of the designated unlabeled RNAs were added, and the mobility of species containing radiolabeled *L23 or *R49 were visualized by autoradiography. Individually, neither *R49 (lanes 1 and 2) nor *L23 (lanes 3 and 4) interacts with A/b′120, while simultaneous presence of R49 and A/b′120 shifts *L23 into dimer (lane 6). L18, an L-module mutant missing the clamping sequence, does not interact with R49 (lane 9) nor does it support dimer formation (lane 8). (C) Determination of $K_d$ using radiolabeled *A/b′120 as a probe. A native gel showed that an increasing amount of dimer was observed as the concentration of unlabeled br-B/a′75 increases, and quantitative analyses of the data presented here yield a $K_d$ value of 58.7 nM for br-B/a′75. (D) Determination of $K_d$ using radiolabeled *L23. Except for the lane where [A/b′120] = 0, each lane contained 0.1 $\mu$M R49 and varying concentrations of A/b′120 as indicated. Bands corresponding to *L23, *br-B/a′, and dimer were observed and quantified. Analyses of the data presented here yielded a $K_d$ value of 68.8 nM.

a′. Furthermore, br-B/a′ was observed to interact with A/b′120 and form a species that has the same mobility as the B/a′75||A/b′120 dimer (Figure 4A, lanes 6 and 7), indicating that the noncovalently linked br-B/a′ RNA is capable of forming pRNA dimers. Individually, neither R49 nor L23 interacted with A/b′120 at concentrations up to 2000 nM (Figure 4B, lanes 1−4). In addition, mixing R49 with L18, a L-loop module mutant missing the clapping duplex sequence, completely destroyed the interaction between the R-loop and L-loop modules, as well as negated dimer formations (Figure 4B, lanes 8−10). Furthermore, experiments showed that a two-piece pRNA derived from the wild-type, full-length pRNA (117 nt) is capable of dimer formation, although the dimer affinity is weakened due to RNA misfolding arisen from the presence of long stretches of clamping sequences corresponding to the full-length DNA translocation domain (supplemental Figure 1, Supporting Information).

To further investigate the br-B/a′ molecule, the $K_d$ between A/b′120 and br-B/a′ was determined utilizing two assays (Figure 4C,D). When radiolabeled *A/b′120 was utilized as the trace component, a $K_d$ value of 48.9 ± 13.8 nM was obtained between *A/b′120 and br-B/a′75 (Figure 4C, Table 2). Alternatively, radiolabeled *L23 was utilized as the trace component (Figure 4D). By adding a constant amount of R49 RNA (0.1 $\mu$M), a fixed amount of *br-B/a′ was formed and utilized as the probe. When dimer formation in the presence of varying concentrations of unlabeled A/b′120 was measured, a $K_d$ value of 68.0 ± 8.2 nM was determined (Figure 4D, Table 2). Within errors, the same $K_d$ values were obtained with different types of trace probe, providing additional support for successful reconstitution of the br-B/a′ species.

The average $K_d$ values measured from the two assays were 58.5 nM for br-B/a′, corresponding to $\Delta G°_{17°C}$ of −9.6 kcal/mol (Table 2). This gave $\Delta\Delta G°_{17°C}$ values of 0.6 kcal/mol,

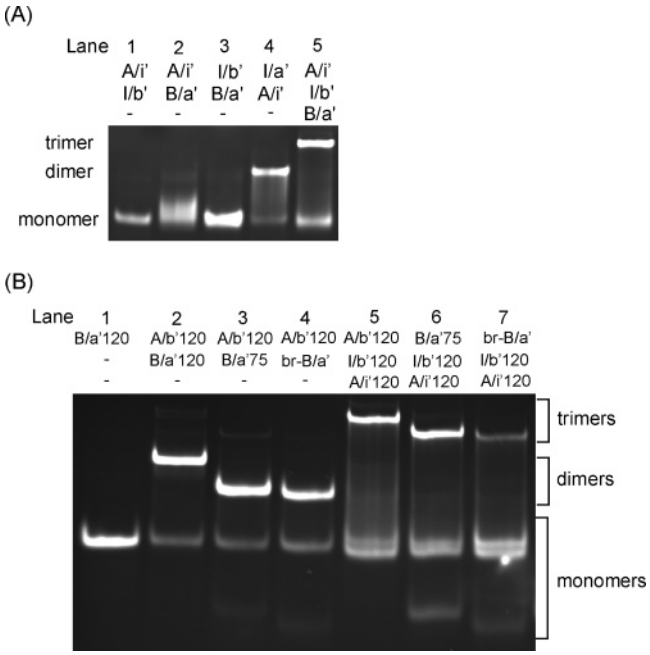


FIGURE 5: Trimer formations under 5 mM $Mg^{2+}$. Each RNA species was 1 $\mu$M. All RNAs were unlabeled, and bands were visualized by ethidium bromide staining. (A) Trimer formations in full-length pRNAs. In lane 5, mixing three pRNAs with the appropriate loop sequences resulted in a band that migrates slower than a dimer (lane 4). Lanes 1−3 show that any two individual pRNAs did not form a stable complex on the native gel. (B) Trimer formations with pRNA variants. Lane 6 showed a trimer formed with B/a′75, which migrates slower than the known dimer species (lane 3). Trimer formation was clearly observed for br-B/a′ (lane 7). The fraction of the trimer complex involving br-B/a′ was reduced. This could arise from entropy effects due to the more flexible nature of the br-B/a′ construct.

as compared to B/a′120, and 0.5 kcal/mol, as compared to B/a′75 (Table 2). These $\Delta\Delta G°_{17°C}$ values are small and indicate that br-B/a′75 maintains a near wild-type ability in forming pRNA dimers. Consistent with this conclusion, competition experiments showed that the br-B/a′ RNA competes handily with the full-length, covalently linked B/a′120 for dimer formation (supplemental Figure 2, Supporting Information). Control experiments also showed that the sequence of the duplex clamp and the absence of the $U_{72}U_{73}U_{74}$ sequence do not influence the measured $K_d$ (supplemental Figure 3, Supporting Information). Taken together, the data suggest a modular architecture of the procapsid binding domain. The R and L submodules, independently synthesized and noncovalently assembled, are capable of folding into an active conformation, where the R and L loops are properly positioned to enable high-affinity interaction with an appropriate pRNA partner.

*Trimer Formations in pRNA Wild-Type and Variants.* Previously, trimer formations with full-length pRNAs have been detected (*22*, *29*). Trimer formations involving B/a′75 and br-B/a′ were studied here to further access how pRNA tertiary folding and interaction are affected by the corresponding mutations. When equal amount of A/i′120, I/b′120, and B/a′120, were mixed, a band corresponding to a pRNA trimer was observed (Figure 5A, lane 5), while combinations of any two individual RNAs show no stable interactions (Figure 5A). When B/a′120 was substituted by B/a′75, a trimer band with lower molecular weight was detected, indicating that B/a′75 is capable of forming trimers, and truncation of the DNA translocation domain does not affect RNA/RNA interaction (Figure 5B, lane 6). Furthermore, br-B/a′ was observed to be active in trimer formation (Figure 5B, lane 7), supporting the conclusion that the noncovalently assembled br-B/a′75 is capable of folding into an active configuration that is functional in intermolecular pRNA/pRNA interaction.

*Accessing the Roles of 2′-Hydroxyl Groups in pRNA Dimer Formation.* The finding that br-B/a′ is fully functional in intermolecular pRNA assembly provides an opportunity to investigate the role of individual RNA functional groups in pRNA structure and interaction. The L23 molecule is easily synthesized using the current technology of solid-phase chemical synthesis, thus, allowing us to introduce site-specific functional group modifications. Measuring the $K_d$ between the mutant br-B/a′ and A/b′120 then provides a way of accessing the effects of such modifications and revealing the role of these functional groups in pRNA tertiary folding and assembly.

The first set of functional groups tested was the 2′-hydroxyl groups within the L-loop. A hybrid dL23 molecule was synthesized, where the four nucleotides in the L-loop were mutated to deoxyribonucleotides (Figure 6A). When dL23 was reconstituted with R49 to form a br-B/*d*a′ species and tested for dimer formation with radiolabeled *A/b′120, less than 30% dimer was observed at br-B/*d*a′ concentrations up to 3000 nM (Figure 6B). The $K_d$ was estimated to be 6885 ± 1584 nM, which is 141-fold weaker than what was measured using the same assay in the all-ribose br-B/a′ (Table 2).

It is possible that high concentrations of unlabeled br-B/*d*a′ (up to 3000 nM) might lead to aberrant interactions, thus, depleting the br-B/*d*a′ molecules that are available for dimer formation and affecting the $K_d$ measurement. This potential problem was avoided when A/b′120 was utilized as the unlabeled, high-concentration species, as studies have shown that A/b′120 does not interact with itself at concentrations as high as 3000 nM (Figure 2A). The $K_d$ between br-B/*d*a′ and A/b′120 was measured again using trace radiolabeled *dL23 as the probe (Figure 6C). A $K_d$ value of 7684 ± 733 nM was obtained, which is close to the value obtained using *A/b′120 as a probe, and 113-fold weaker than what was measured using the same assay in the br-B/a′ system (Table 2).

The average $K_d$ value measured from the two assays was 7285 nM for br-B/da′. This corresponds to $\Delta G°_{17°C}$ of −7.1 kcal/mol, which is 3.4 kcal/mol weaker than that of the wild-type full-length pRNA (Table 2). Compared to br-B/a′ ($<K_d> = 58.5$ nM), deleting the four 2′-hydroxyl groups in one of the L-loops weakens the dimer affinity by 125-fold, which corresponds to a $\Delta\Delta G°_{17°C}$ of 2.8 kcal/mol. This indicates that the missing 2′-hydroxyl groups significantly affect dimer formation.

## DISCUSSION

*Modular Architecture of the Procapsid Binding Domain.* Data presented here suggest that the procapsid binding domain is constituted of two modules: an R module that encompasses the R-loop and an L module that encompasses the L-loop. The two submodules can be independently synthesized. Under functional $Mg^{2+}$ concentrations, the R

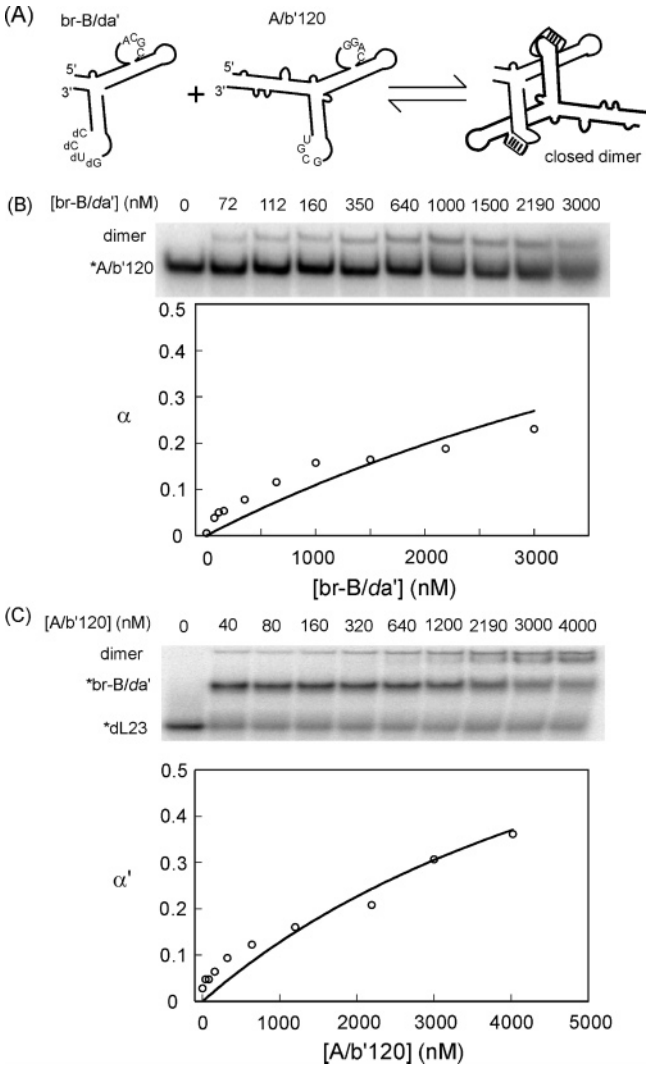


FIGURE 6: Dimer formation with the br-B/*da*′ pRNA, where deoxyribonucleotides were substituted in one of the L-loops. (A) A schematic representation showing the L-loop sequence and the secondary structure of the br-B/*da*′ molecule and its interaction with the partner A/b′120 RNA. (B) Determination of $K_d$ using radiolabeled *A/b′120 as a probe. Data presented here yielded an estimated $K_d$ value of 8134 nM. (C) Determination of $K_d$ using radiolabeled *dL23. Except for the lane where [A/b′120] = 0, each lane contained 0.1 $\mu$M R49 and varying concentrations of A/b′120 as indicated. Controls showed that, in the absence of R49, *dL23 does not interact with A/b′120 at a concentration up to 3000 nM. Bands corresponding to *dL23, *br-B/a′, and dimer were observed and quantified. Data presented here yielded an estimated $K_d$ value of 6837 nM.

and L modules interact noncovalently and fold into a conformation where the R-loop and the L-loop are properly positioned for full activity in both dimer and trimer formation. It has been shown that the pRNA procapsid binding domain and the DNA translocation domain function independently (*5*, *6*), and data presented here provide evidence that the procapsid binding domain can be dissected into two physically separate modules. Together, this leads to a model that describes a pRNA monomer as three arms spanning a hinge, with arm 1 encompassing the DNA translocation domain, arm 2 encompassing the R-loop, and arm 3 encompassing the L-loop (Figure 7A).

The simple three-arms-around-a-hinge model serves as a general framework for probing the pRNA structure and

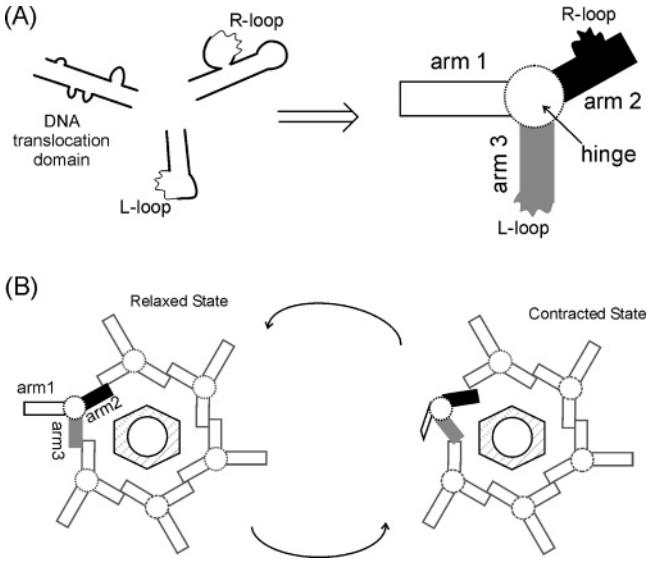


FIGURE 7: A model for pRNA structure and function. (A) A schematic representation of the three-arms-around-a-hinge model. The three modules of a pRNA monomer are shown schematically on the left. These are simplified as three arms (arm1, white; arm2, black; and arm3, gray) assembled around the central loop acting as a hinge (dotted line). (B) A possible model for pRNA function. As shown, pRNAs bind to procapsid (shaded hexagon) and form a hexameric ring. ATP hydrolysis causes relative movements between arms 1, 2, and 3 in a monomer (indicated by dark line), and leads it into the contracted state. Such motions in the active monomer enable arm 1 motions that directly or indirectly translocate DNA. The pRNA monomers alternate between the relaxed/contracted states sequentially and enable DNA packaging.

understanding the mode of pRNA conformational changes. For example, pRNA might function through relative motions between the arms. It is interesting that the proposed arm 2 contains a reported ATP-binding region (*26*), and it is possible that ATP binding and hydrolysis in one RNA monomer might cause conformational changes in arm 2 (Figure 7B). This could lead to swinging of arm 1 that might translocate DNA either directly or through protein action. Conformational changes in arm 2 also might induce a tweezer-like motion between arm 2 and arm 3, thus, leading the active monomer to a contracted state to drive the proposed rotation of the motor complex (*9*, *10*, *41*). Motion in arm 3 consequently might dispatch arm 2 of the next pRNA and transmits the signal for the next RNA to fire, thus, accounting for the proposed sequential action model for pRNA functions (*8*). Formulating branched RNA systems as rigid body arms and hinges has been reported in studies of other RNA systems (*42*−*49*). While much more in-depth studies are required to unveil the mechanism of pRNA function and DNA translocation, results presented here lay the foundation for further biophysical and biochemical studies that will reveal the detailed structure of each arm (each module) and relative orientations between the arms. This will aid in delineating the mechanism of pRNA function during DNA packaging.

In this study, the folding of a pRNA molecule was assessed through its ability to participate in pRNA interaction, namely, forming dimers and trimers. The data indicate that the reconstituted two-piece br-B/a′ molecule is capable of dimer and trimer formation, thus, meeting a necessary criterion for being an active pRNA. The br-B/a′ construct is highly versatile in controlling pRNA/pRNA interactions; for ex-

ample, one can now tune the affinity of pRNA dimers by manipulating the L-loop 2′-OH groups. In the absence of proteins, pRNA dimers and trimers have been utilized to construct novel nanostructures and to deliver gene therapy agents (*27*−*29*). Studies reported here offer insights into pRNA structural organization, as well as expand our capability in manipulating pRNA/pRNA interactions. These are advantageous for developments of pRNA-based technology. Furthermore, previous studies have revealed overlapping requirements for pRNA/pRNA interaction and pRNA/procapsid interaction (*22*). It remains to be tested whether the two-piece br-B/a′ molecule is active in interacting with the procapsid and whether the modular organization of the procapsid binding domain is maintained throughout its function during motor function.

To construct the two-piece br-B/a′, the boundary between the R-loop module and the L-loop module has been chosen to be the $U_{72}U_{73}U_{74}$ loop. This is consistent with previous studies indicating that the $U_{72}U_{73}U_{74}$ loop is a point of flexibility (*16*, *35*). There might exist multiple locations at which loss of covalent linkage has no effect on the tertiary structure and activity of the procapsid binding domain. In addition, data presented here show that the R and L modules could not assemble without the clamping duplex, suggesting a lack of extensive, high-affinity interactions between these two modules. This is consistent with previous photocross-linking investigations that detected only limited cross-links within the procapsid binding domain (*32*). The fact that the R and L modules do not dock with each other strongly might facilitate pRNA conformational changes during packaging motor function.

*L-Loop 2′-Hydroxyl Groups Affect Procapsid Binding Domain Folding and Interaction.* What elements control the correct positioning of the R and L loops and ensure high affinity in pRNA/pRNA interaction? Currently available data suggest that these elements do not reside within the DNA translocation domain, because mutations in this region do not affect pRNA/pRNA interactions (see reviews *5*, *6*, Figure 3). Within the procapsid binding domain, probable regions where these controlling elements exist are the R and L loops. Extensive investigations have shown that pRNA/pRNA interaction and packaging motor function rely on only base complementarity, not base sequence, between the R-loop and the L-loop (see reviews *5*, *6*). This strongly suggests that base functional groups within the R-loop and the L-loop are unlikely to participate in additional tertiary interactions that are critical for pRNA folding and interaction. However, until now, there is no information on the role of nonbase functional groups in pRNA interaction and function.

Constructs reported here enable us to study, for the first time, nonbase functional groups that control procapsid binding domain folding and interaction. Data reported here indicate that, under $Mg^{2+}$ concentration at which the DNA packaging motor function is usually assayed (*18*, *19*), deleting the 2′-hydroxyl groups in one of the L-loops weakens the pRNA dimer affinity by 125-fold, which corresponds to a $\Delta\Delta G^{\circ}_{17^{\circ}C}$ of 2.8 kcal/mol. While only the 2′-hydroxyl groups in one L-loop were tested, symmetry constraints dictate that the same conclusion is applicable to both L-loops.

In all current pRNA structure models, the R/L interaction is treated as a simple RNA duplex (*19*, *23*, *34*). Deleting the 2′-hydroxyl groups in the L-loop changes one of the R/L interactions to a DNA/RNA hybrid, which is known to be weaker than an RNA/RNA duplex with the same sequence. Calculations of duplex stability according to the well-established nearest neighbor model were carried out on duplexes with the A||a′ sequence using thermodynamic parameters reported in the literature. The $\Delta G^{\circ}_{17^{\circ}C,duplex}$ was calculated to be −5.7 kcal/mol for an RNA/RNA duplex (A||a′) (*50*) and −4.4 kcal/mol for an RNA/DNA hybrid (A||da′) (*51*). Although these values were calculated using parameters measured at 1.0 M NaCl, studies have shown that these parameters can be used to predict duplex stability in the presence of a few millimolar of $Mg^{2+}$ (*50*) (P.Z.Q., data not shown) and therefore is applicable in studies reported here. Assuming that the A||a′ interaction can be modeled as an RNA duplex, the calculated $\Delta\Delta G^{\circ}_{17^{\circ}C,duplex}$ is 1.3 kcal/mol between a DNA/RNA hybrid and the corresponding RNA/RNA duplex, corresponding to a ratio of 9.2 in $K_d$ values at 17 °C. This leaves 1.5 kcal/mol of destabilization energy in pRNA dimer formation that cannot be accounted for by local duplex deformation.

Because the affinity in forming the dimer is linked directly to the folding of the individual pRNAs and the correct positioning of the R and L loops, destabilization in dimer stability beyond the degree due to local duplex deformation likely indicates that one or more 2′-hydroxyl groups in the L-loop play a significant and specific role in the folding and interaction of the procapsid binding domain. Ample examples have been documented for the participation of 2′-hydroxyl groups in RNA structure and interaction. Particularly, 2′-hydroxyl groups have been shown to mediate tertiary interactions and catalysis via hydrogen bonding (*52*−*58*), to coordinate metal ion binding (*59*−*62*), and to contribute to protein or solvent interactions (*63*−*65*). It is possible that one or more of these 2′-hydroxyl groups in the L-loop of a pRNA form critical intramolecular tertiary contacts to other regions of the pRNA, thus, contributing to the proper folding of the procapsid binding domain and the correct positioning of the R and L loops. We note that the energetic contribution from these 2′-hydroxyl groups is significant yet not excessive, which is consistent with a lack of strong tertiary docking interactions between the two sub-modules within the procapsid binding domain (vide supra). These 2′-hydroxyl groups might also form intermolecular contacts to the partner pRNA, which would directly contribute to dimer affinity. In addition, it remains possible that helical deformation in the R/L interaction might propagate to other regions of pRNA and affect dimer stability.

Data reported here are the initial indication that nonbase functionalities participate in structure and function of pRNA. In the future, single 2′-hydroxyl substitutions within the L-loop will be carried out to reveal the exact identity of the 2′-hydroxyl group(s) that affects the dimer affinity. A similar methodology will be applied to study the role of other functional groups in the interacting loop region, as well as other regions of pRNA. Involvement of RNA functional groups in pRNA/protein interactions will also be investigated. These studies will allow us to identify critical functional groups, to reveal essential tertiary interactions, and to provide much needed structural constraints in studies of pRNA structure and function.

*Perspectives.* Identifying the autonomous units within the procapsid binding domain supports a modular organization

of pRNA and has led to a general framework for probing pRNA conformations. The functional two-piece br-B/a′ system renders it possible to probe essential functional groups and tertiary interactions that maintain structure and function of the procapsid binding domain. The br-B/a′ system is also more amendable to biophysical studies, such as NMR (*66*), fluorescence spectroscopy (*67*), and the recently developed site-directed spin labeling (*66*, *68*−*70*). These studies will provide important information on the pRNA structure, aid in developments of pRNA based technology, and greatly impact our understanding of pRNA and DNA packaging motor function.

## ACKNOWLEDGMENT

We thank Dr. Peixuan Guo for kindly providing the pT7temp plasmid, Dr. Anna M. Pyle for critical reading of the manuscript, and a reviewer for suggestions on the significance of pRNA in nanotechnology and gene therapy developments.

## SUPPORTING INFORMATION AVAILABLE

Dimer formation of various two-piece pRNA constructs and competition between br-B/a′ and B/a′120. This material is available free of charge via the Internet at http://pubs.acs.org.

## REFERENCES

1. Black, L. W. (1989) DNA packaging in dsDNA bacteriophages, *Annu. Rev. Microbiol. 43*, 267−292.
2. Valpuesta, J. M., and Carrascosa, J. L. (1994) Structure of viral connectors and their function in bacteriophage assembly and DNA packaging, *Q. Rev. Biophys. 27*, 107−155.
3. Fujisawa, H., and Morita, M. (1997) Phage DNA packaging, *Genes Cells 2*, 537−545.
4. Catalano, C. E. (2000) The terminase enzyme from bacteriophage lambda: a DNA-packaging machine, *Cell. Mol. Life Sci. 57*, 128−148.
5. Grimes, S., Jardine, P. J., and Anderson, D. (2002) Bacteriophage phi29 DNA packaging, *Adv. Virus Res. 58*, 255−294.
6. Guo, P. (2002) Structure and function of $\phi$29 hexameric RNA that drives the viral DNA packaging motor: Review, *Prog. Nucleic Acids Res. Mol. Biol. 72*, 415−473.
7. Smith, D. E., Tans, S. J., Smith, S. B., Grimes, S., Anderson, D. L., and Bustamante, C. (2001) The bacteriophage phi29 portal motor can package DNA against a large internal force, *Nature 413*, 748−752.
8. Chen, C., and Guo, P. (1997) Sequential action of six DNA-packing pRNAs during phage $\phi$29 genomic DNA translocation, *J. Virol. 71*, 3864−3871.
9. Simpson, A. A., Tao, Y., Leiman, P. G., Badasso, M. O., He, Y., Jardine, P. J., Olson, N. H., Morals, M. C., Grimes, S., Anderson, D. L., Baker, T. S., and Rossmann, M. G. (2000) Structure of the bacteriophage phi29 DNA packaging motor, *Nature 408*, 745−750.
10. Guasch, A., Pous, J., Ibarra, B., Gomis-Ruth, F. X., Valpuesta, J. M., Sousa, N., Carrascosa, J. L., and Coll, M. (2002) Detailed architecture of a DNA translocating machine: the high-resolution structure of the bacteriophage phi29 connector particle, *J. Mol. Biol. 315*, 663−676.
11. Serwer, P. (2003) Models of bacteriophage DNA packaging motors, *J. Struct. Biol. 141*, 179−188.
12. Guo, P., Erickson, S., and Anderson, D. (1987) A small viral RNA is required for in vitro packaging of bacteriophage $\phi$29 DNA, *Science 236*, 690−694.
13. Reid, R. J. D., Zhang, F., Benson, S., and Anderson, D. (1994) Identification of bacteriophage $\phi$29 prohead RNA domains necessary for in vitro DNA-gp3 packaging, *J. Biol. Chem. 269*, 9084−9089.
14. Zhang, C. L., Lee, C.-S., and Guo, P. (1994) The proximate 5′ and 3′ ends of the 120-base viral RNA (pRNA) are crucial for the packaging of bacteriophage $\phi$29 DNA, *Virology 201*, 77−85.
15. Reid, R. J. D., Bodley, J. W., and Anderson, D. (1994) Characterization of the prohead-pRNA interaction of bacteriophage $\phi$29, *J. Biol. Chem. 269*, 5157−5162.
16. Reid, R. J. D., Zhange, F., Benson, S., and Anderson, D. (1994) Probing the structure of the bacteriophage $\phi$29 prohead RNA with specific mutations, *J. Biol. Chem. 269*, 18656−18661.
17. Garver, K., and Guo, P. (1997) Boundary of pRNA functional domains and minimum pRNA sequence requirement for specific connector binding and DNA packaging of phage $\phi$29, *RNA 3*, 1068−1079.
18. Guo, P., Zhang, C., Chen, C., Garver, K., and Trottier, M. (1998) Inter-RNA interaction of phage $\phi$29 pRNA to form a hexameric complex for viral DNA transportation, *Mol. Cell 2*, 149−155.
19. Zhang, F., Lemieux, S., Wu, X., St.-Arnaud, D., McMurray, C. T., Major, F., and Anderson, D. (1998) Function of hexameric RNA in packaging of bacteriophage $\phi$29 DNA in vitro, *Mol. Cell 2*, 141−147.
20. Chen, C. P., Zhang, C. L., and Guo, P. (1999) Sequence requirement for hand-in-hand interaction in formation of pRNA dimers and hexamers to gear phi29 DNA translocation motor, *RNA 5*, 805−818.
21. Trottier, M., Mat-Arip, Y., Zhang, C. L., Chen, C. P., Sheng, S., Shao, Z., and Guo, P. (2000) Probing the structure of the monomers and dimers of the bacterial virus phi29 hexamer RNA complex by chemical modification, *RNA 6*, 1−10.
22. Chen, C. P., Sheng, S., Shao, Z., and Guo, P. (2000) Dimer as a building block in assembling RNA, *J. Biol. Chem. 275*, 17510−17516.
23. Hoeprich, S., and Guo, P. (2002) Computer modeling of three-dimensional structure of DNA-packaging RNA (pRNA) monomer, dimer, and hexamer of phi29 DNA packaging motor, *J. Biol. Chem. 23*, 20794−20804.
24. Ibarra, B., Caston, J. R., Llorca, O., Valle, M., Valpuesta, J. M., and Carrascosa, J. L. (2000) Topology of the components of the DNA packaging machinery in the phage $\phi$29 prohead, *J. Mol. Biol. 298*, 807−815.
25. Grimes, S., and Anderson, D. (1990) RNA dependence of the bacteriophage phi29 DNA packaging ATPase, *J. Mol. Biol. 215*, 559−566.
26. Shu, D., and Guo, P. (2003) A viral RNA that binds ATP and contains a motif similar to an ATP-binding aptamer from SELEX, *J. Biol. Chem. 278*, 7119−7125.
27. Hoeprich, S., Zhou, Q., Guo, S., Shu, D., Qi, G., Wang, Y., and Guo, P. (2003) Bacterial virus phi29 pRNA as a hammerhead ribozyme escort to destroy hepatitis B virus, *Gene Ther. 10*, 1258−1267.
28. Shu, D., Moll, W., Deng, Z., Mao, C., and Guo, P. (2004) Bottom-up assembly of RNA arrays and superstructures as potential parts in nanotechnology, *Nano Lett. 4*, 1717−1723.
29. Shu, D., Huang, L. P., Hoeprich, S., and Guo, P. (2003) Construction of phi29 DNA-packaging RNA monomers, dimers, and trimers with variable sizes and shapes as potential parts for nanodevices, *J. Nanosci. Nanotechnol. 3*, 295−302.
30. Chen, C., and Guo, P. (1997) $Mg^{2+}$-induced conformational change of packaging RNA for procapsid recognition and binding during phage $\phi$29 DNA encaspsidation, *J. Virol. 71*, 495−500.
31. Zhang, C., Trottier, M., Chen, C., and Guo, P. (2001) Chemical modification patterns of active and inactive as well as procapsid-bound and unbound DNA-packaging RNA of baterial virus phi29, *Virology 281*, 281−293.
32. Mat-Arip, Y., Garver, K., Chen, C., Sheng, S., Shao, Z., and Guo, P. (2001) Three-dimensional interaction of phi29 pRNA dimer probed by chemical modification interference, cryo-AFM, and cross-linking. *J. Biol. Chem. 276*, 32575−32584.
33. Mohammad, T., Chen, C., Guo, P., and Morrison, H. (1999) Photoinduced cross-linking of RNA by cis-Rh(phen)2Cl2+ and cis-Rh(phen)(phi)Cl2+: a new family of light activatable nucleic acid cross-linking agents. *Bioorg. Med. Chem. Lett. 9*, 1703−1708.
34. Bourassa, N., and Major, F. (2002) Inplication of the prohead RNA in phage phi29 DNA packaging, *Biochimie 84*, 945−951.
35. Zhang, C. L., Tellinghuisen, T., and Guo, P. (1997) Use of circular permutation to assess six bulges and four loops of DNA-packaging pRNA of bacteriophage $\phi$29, *RNA 3*, 315−323.

36. Davanloo, P., Rosenberg, A. H., Dunn, J. J., and Studier, W. F. (1984) Cloning and expression of the gene for bacteriophage T7 RNA polymerase, *Proc. Natl. Acad. Sci. U.S.A. 81*, 2035−2039.
37. Pyle, A. M., and Green, J. B. (1994) Building a kinetic framework for group II intron ribozyme activity: quantitation of interdomain binding and reaction rate, *Biochemistry 33*, 2716−2725.
38. Milligan, J. F., and Uhlenbeck, O. C. (1989) Synthesis of small RNAs using T7 RNA polymerase, *Methods Enzymol. 180*, 51−62.
39. Griffin, E. A., Qin, Z., Michels, W. J., and Pyle, A. M. (1995) Group II intron ribozymes that cleave DNA and RNA linkages with similar efficiency, and lack contacts with substrate 2′-hydroxyl groups, *Chem. Biol. 2*, 761−770.
40. Gish, G., and Eckstein, F. (1988) DNA and RNA sequence determination based on phosphorothioate chemistry, *Science 240*, 1520−1522.
41. Hendrix, R. W. (1978) Symmetry mismatch and DNA packaging in large bacteriophages, *Proc. Natl. Acad. Sci. U.S.A. 75*, 4779−4783.
42. Gohlke, C., Murchie, A. I., Lilley, D. M., and Clegg, R. M. (1994) Kinking of DNA and RNA helices by bulged nucleotides observed by fluorescence resonance energy transfer, *Proc. Natl. Acad. Sci. U.S.A. 91*, 11660−11664.
43. Tuschl, T., Gohlke, C., Jovin, T., Westhof, E., and Eckstein, F. (1994) A three-dimensional model for the hammerhead ribozyme based on fluorescence measurements, *Science 266*, 785−789.
44. Walter, F., Murchie, A. I., Duckett, D. R., and Lilley, D. M. (1998) Global structure of four-way RNA junctions studied using fluorescence resonance energy transfer, *RNA 4*, 719−728.
45. Murchie, A. I., Thomson, J. B., Walter, F., and Lilley, D. M. (1998) Folding of the hairpin ribozyme in its natural conformation achieves close physical proximity of the loops, *Mol. Cell 1*, 873−881.
46. Walter, N. G., Burke, J. M., and Millar, D. P. (1999) Stability of hairpin ribozyme tertiary structure is governed by the interdomain junction, *Nat. Struct. Biol. 6*, 544−549.
47. Klostermeier, D., and Millar, D. P. (2000) Helical junctions as determinants for RNA folding: origin of tertiary structure stability of the hairpin ribozyme, *Biochemistry 39*, 12970−12978.
48. Orr, J. W., Hagerman, P. J., and Williamson, J. R. (1998) Protein and Mg(2+)-induced conformational changes in the S15 binding site of 16 S ribosomal RNA, *J. Mol. Biol. 275*, 453−464.
49. Lafontaine, D. A., Norman, D. G., and Lilley, D. M. (2002) The global structure of the VS ribozyme, *EMBO J. 21*, 2461−2471.
50. Xia, T., SantaLucia, J. J., Burkard, M. E., Kierzek, R., Schroeder, S. J., Jiao, X., Cox, C., and Turner, D. H. (1998) Thermodynamic parameters for an expanded nearest-neighbor model for formation of RNA duplexes with Watson−Crick base pairs, *Biochemistry 37*, 14719−14735.
51. Sugimoto, N., Nakano, S., Katoh, M., Matsumura, A., Nakamuta, H., Ohmichi, T., Yoneyama, M., and Sasaki, M. (1995) Thermodynamic parameters to predict stability of RNA/DNA hybrid duplexes, *Biochemistry 34*, 11211−11216.
52. Pyle, A. M., and Cech, T. R. (1991) Ribozyme recognition of RNA by tertiary interactions with specific ribose 2′-OH groups, *Nature 350*, 628−631.
53. Herschlag, D., Eckstein, F., and Cech, T. R. (1993) The importance of being ribose at the cleavage site in the *Tetrahymena* ribozyme reaction, *Biochemistry 32*, 8312−8321.
54. Herschlag, D., Eckstein, F., and Cech, T. R. (1993) Contributions of 2′-hydroxyl groups of an RNA substrate to binding and catalysis by the *Tetrahymena* ribozyme. An energetic picture of an active site composed of RNA, *Biochemistry 32*, 8299−8311.
55. Abramovitz, D. L., Friedman, R. A., and Pyle, A. M. (1996) Catalytic role of 2′-hydroxyl groups within a group II intron active site, *Science 271*, 1410−1413.
56. Silverman, S. K., and Cech, T. R. (1999) Energetics and cooperativity of tertiary hydrogen bonds in RNA structure, *Biochemistry 38*, 8691−8702.
57. Klostermeier, D., and Millar, D. P. (2002) Energetics of hydrogen bond networks in RNA: hydrogen bonds surrounding G+1 and U42 are the major determinants for the tertiary structure stability of the hairpin ribozymes, *Biochemistry 41*, 14095−14102.
58. Schwans, J. P., Cortez, C. N., Olvera, J. M., and Piccirilli, J. A. (2003) 2′-Mercaptonucleotide interference reveals regions of close packing within the folded RNA molecules, *J. Am. Chem. Soc. 125*, 10012−10018.
59. Smith, D., and Pace, N. R. (1993) Multiple magnesium ions in the ribonuclease P reaction mechanism, *Biochemistry 32*, 5273−5281.
60. Cate, J. H., Hanna, R. L., and Doudna, J. A. (1997) A magnesium ion core at the heart of a ribozyme domain, *Nat. Struct. Biol. 4*, 553−558.
61. Shan, S., and Herschlag, D. (1999) Probing the role of metal ions in RNA catalysis: kinetic and thermodynamic characterization of a metal ion interaction with the 2′-moeity of the guanosine nucleophile in the *Tetrahymena* group I ribozyme, *Biochemistry 38*, 10958−10975.
62. Gordon, P. M., Sontheimer, E. J., and Piccirilli, J. A. (2000) Kinetic characterization of the second step of group II intron splicing: role of metal ions and the cleavage site 2′-OH in catalysis, *Biochemistry 39*, 12939−12952.
63. Egli, M., Portmann, S., and Usman, N. (1996) RNA hydration: a detailed look, *Biochemistry 35*, 8489−8494.
64. Hou, Y., Zhang, X., Holland, J. A., and Davis, D. R. (2001) An important 2′-OH group for an RNA-protein interaction, *Nucleic Acids Res. 29*, 976−985.
65. Dertinger, D., Dale, T., and Uhlenbeck, O. C. (2001) Modifying the specificity of an RNA backbone contact, *J. Mol. Biol. 314*, 649−654.
66. Qin, P. Z., and Dieckmann, T. (2004) Application of NMR and EPR methods to the study of RNA, *Curr. Opin. Struct. Biol. 14*, 350−359.
67. Walter, N. G., Harris, D. A., Pereira, M. J., and Rueda, D. (2002) In the fluorescent spotlight: global and local conformational changes of small catalytic RNAs, *Biopolymers 61*, 224−242.
68. Qin, P. Z., Butcher, S. E., Feigon, J., and Hubbell, W. L. (2001) Quantitative analysis of the GAAA tetraloop/receptor interaction in solution: a site-directed spin labeling study, *Biochemistry 40*, 6929−6936.
69. Edwards, T. E., Okonogi, T. M., Robinson, B. H., and Sigurdsson, S. T. (2001) Site-specific incorporation of nitroxide spin-labels into internal sites of the TAR RNA. Structure-dependent dynamics of RNA by EPR spectroscopy, *J. Am. Chem. Soc. 123*, 1527−1528.
70. Qin, P. Z., Hideg, K., Feigon, J., and Hubbell, W. L. (2003) Monitoring RNA base structure and dynamics using site-directed spin labeling, *Biochemistry 42*, 6772−6783.

BI0475020